NPG Asia Materials (2013) 5, e38; doi:10.1038/am.2013.1

www.nature.com/am

ORIGINAL ARTICLE

Single ferroelectric-domain photovoltaic switch based on lateral $BiFeO_3$ cells

Ji Ho Sung[1], Won-Mo Lee[2,3], Jin Hong Lee[4], Kanghyun Chu[4], Donghun Lee[3], Xavier Moya[5], Neil D Mathur[5], Chan-Ho Yang[4], Jae-Hoon Park[1] and Moon-Ho Jo[3]

The bistability of ferroelectric polarization states serves as a basis for solid-state memory. This phenomenon can also yield an interesting photovoltaic effect in such a way that the directional photocarrier motion follows the inherent potential gradient imposed by the ferroelectric polarization vectors. Here, we demonstrate a single-domain photovoltaic switch based on lateral $BiFeO_3$ channels, in which such photovoltaic switching is achieved by a coherent single-domain reversal with a short electrical pulse. We then provide visual evidence for such operations with a series of spatially and spectrally resolved short-circuit photocurrent images. Specifically, we reveal that the sequential photovoltaic current images directly reflect the remanent polarization states of a single-domain channel. We also verify that, in multidomain channels, diffusive switching characteristics are determined not only by the internal polarization vector within the domain but also by oxygen vacancy accumulation at the domain walls.

NPG Asia Materials (2013) **5,** e38; doi:10.1038/am.2013.1; published online 8 February 2013

Keywords: ferroelectrics; multiferroics; oxide photonics; photovoltaics

INTRODUCTION

Homogeneous light illumination on non-centrosymmetric crystals, such as ferroelectrics, in the intrinsic absorption range can give rise to an interesting photovoltaic effect, dubbed as the bulk photovoltaic effect.[1,2] This effect is distinct from that of typical semiconductor p–n junction photovoltaics and excitonic heterojunction photovoltaics in that the photogenerated carriers can be separated along the inherent polar directions, ensuing the unidirectional photocurrent (I_{ph}) and photovoltage (V_{ph}), associated with the spontaneous ferroelectric polarization vector ($\boldsymbol{P}_s$). Therein, the open-circuit voltage (V_{oc}) is determined by the magnitude of the remanent polarization of ferroelectrics, and it can be additively as large as a few hundreds of volts, although the short-circuit current ($I_{sc} \equiv I_{ph}$ at 0 V) is low due to the insulating character of the system. This phenomenon has been recently revisited with a small band-gap, $BiFeO_3$ (BFO) ferroelectric, from which a substantially higher photon-to-charge generation efficiency can be achieved in the visible range compared with that of other insulating ferroelectrics.[3–8] Choi *et al.*[3] reported that diode-like rectification follows the polarization-dependent interface band-bending of BFO single-crystal slabs that are electrically switchable, that is, V_{oc} and I_{sc} are defined by the remanent polarization directions. In general, the spatial extent of spontaneous polarization vectors in ferroelectric crystals is typically manifested as domains (typically spanning over a few μm in size) and domain walls (DW, 1–2 nm in width), which must intimately determine the polarization-switching characteristics in a ferroelectric continuum.[1–4,8–10] In this study, we demonstrate a single-domain photovoltaic switch based on a lateral BFO channel with voltage pulses, in which coherent switching is achieved on a time scale as fast as 10 μs. By employing spatially and spectrally resolved I_{ph} imaging on a single domain, we provide direct evidence that the photovoltaic switching characteristics are determined by the internal polarization vector along the applied electrical field (*E*-field). In addition, in multidomain channels, we show that oxygen vacancy accumulation at the domain walls (DWs), characteristic of perovskite oxides, is intimately associated with the diffusive switching characteristics. Our study holds general implications for the design rules of ferroelectric photovoltaic cells, which can be tuned by domain engineering and nano-ionic transport.

MATERIALS AND METHODS

We prepared two different types of rhombohedral BFO thin film channels, in which the initial domain structures were a single domain and multiple domains, as shown in the in-plane domain images of Figures 1a and b. These distinct domain structures are established by the heteroepitaxial relationship between (001)-oriented epitaxial BFO thin films on (001) and (110) $SrTiO_3$ substrates[11,12]; note that we used the pseudocubic cell notation for rhombohedral BFO thin films. While the (110) BFO shown in Figure 1a maintains a single-domain texture, the (100) BFO shown in Figure 1b exhibits

[1]Division of Advanced Materials Science, Pohang University of Science and Technology (POSTECH), Pohang, Gyungbuk, Korea; [2]Department of Materials Science and Engineering, Pohang University of Science and Technology (POSTECH), Pohang, Gyungbuk, Korea; [3]Department of Materials Science and Engineering, Yonsei University, Seoul, Korea; [4]Department of Physics, Kaist, Korea and [5]Department of Materials Science, University of Cambridge, Cambridge, UK
Correspondence: Professor M-H Jo, Department of Materials Science and Engineering, Yonsei University, 50 Yonsei-Ro, Seodaemun-Gu, Seoul 120-749, Korea.
E-mail: mhjo@yonsei.ac.kr
Received 1 November 2012; revised 5 December 2012; accepted 6 December 2012

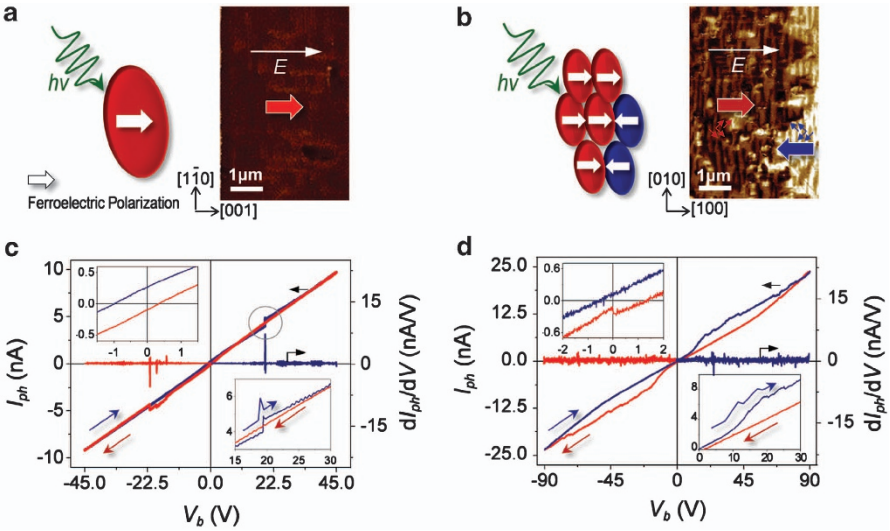

Figure 1 (**a**, **b**) Schematics of photovoltaic measurements conducted in this study and in-plane piezoresponse force microscope (PFM) images of (110) BFO single domain and (100) BFO multidomains, where the net polarization directions are indicated by red and blue arrows. The in-plane PFM images were obtained after the 90 V poling, as indicated by white arrows. (**c**, **d**) The corresponding I_{ph}-V characteristics under global illumination on single-domain (**c**) and multidomain (**d**) BFO cells. The derivatives of I_{ph} with respect to V are also plotted. The lower right insets show the variation of the transient current associated with the switching characteristics of each domain. The upper left insets are magnified views of the low E-field region, showing photovoltaic effects.

striped domains lying along the <010> direction with the two variants in the [110] and [11-0] directions across the 71° or 109° DWs.[13,14] Out-of-plane PFM measurements (not shown) confirmed that the out-of-plane components are pointing downward, that is, from the surface to the substrate. The rectangular device channels were defined by an electrode gap of 4 μm and a width of 30 μm by e-beam lithography and Au-electrode liftoff. Spatially resolved I_{ph} mapping was performed using a focused 532 nm laser with a diameter of 500 nm.[15,16] While continuously varying the in-plane position of the BFO channel using a nanometer-scale controllable piezo scanner, the I_{sc} was lock-in measured as a function of the laser illumination position at the excitation frequency of 100 Hz, relayed by the optical chopper placed between the laser source and the BFO channel.

RESULTS AND DISCUSSION

Figures 1c and d illustrate the I_{ph}–V characteristics under global light illumination on a single domain and multiple domains of BFO at a V sweep rate of 9 V min^{-1}. First, we immediately notice that the I_{ph}–V curves are hysteretic, with a linear background slope of a few MΩ cm of resistivity, upon each domain-reversal process. This observation represents a transient current characteristic in ferroelectrics that is associated with the capacitance change at the electrode contacts due to the net polarization variation under an applied E-field.[17] While the I_{ph} increases upon a single abrupt switching in the single domain BFO marked by a circle, as shown clearly in the lower right inset of Figure 1c, it increases in continuous minute steps for the multidomains, as shown in the lower right inset of Figure 1d, reminiscent of the Barkhausen effects of magnetization processes. Second, as shown in the upper left insets of Figures 1c and d, these features commonly exhibit a photovoltaic effect in the low-E-field region, consistent with the literature.[3–8] Figures 2a and d show the in-plane domain images and the corresponding I_{sc} images for single-domain switching. In the intermediate reversal field, as in the domain image of E_{poling} at +45 V and the I_{sc} image at −20 V, the domain breaks up into two subdomains, showing signs of I_{sc} to each other. Such a one-to-one correspondence clearly demonstrates that the I_{ph} direction is directly determined by the $\boldsymbol{P}_S$ vector configuration, which can be switched by the applied E-field, following the photovoltaic switching of a single domain. Meanwhile, in the multidomain channel, switching gradually proceeds via multidomain switching[18] as shown in Figure 2b, giving rise to a diffusive transition in a series of I_{sc} images as a function of the poling field in Figure 2e, where the direction and magnitude of the local $\boldsymbol{P}_S$ is particularly intermixed in the intermediate field. Figure 2c shows the total I_{sc} magnitude, which was measured under global light illumination over the entire channel, as a function of the poling field; it is reminiscent of the typical polarization hysteresis of ferroelectrics. Essentially, the shape of the hysteresis loop represents the remanent polarization states during E-poling. These observations indicate that the ferroelectric photovoltaics directly follow the local polarization states and their switching characteristics.

The single-domain switching of BFO ferroelectrics can also be induced by a short electrical pulse. Figures 3a and b show the induced I_{ph} variation under continuous light illumination in a single domain channel by a train of square voltage pulses. The sign and magnitude of the I_{ph} immediately change upon applying an input voltage of ±90 V in a reproducible manner over more than a few thousand repetitions. As in Figure 3c, coherent switching was observed at a pulse width as narrow as 10 μs, which is limited by our measurement instruments, not by the intrinsic switching dynamics of BFO on the nanosecond scale.[19] The insets of the I_{sc} images at each pulse width confirm that the photovoltaic switching is highly stable, with its spatial uniformity extending over the range of the pulse width, due to the coherent polarization states generated during single-domain switching. In the multidomain channel, however, we were not able to induce stable switching with square pulses (not shown). Rather, it was only possible by applying a continuous DC voltage sweep up to ±90 V at a moderate sweep rate.

Figures 4a and b show the switchable photovoltaic characteristics for the single- and multidomain channels in the low-E-field range after a *DC* voltage poling of ±90 V. Notably, in the multidomain channels, I_{ph} (thus I_{sc}) increases until reaching a value five times that

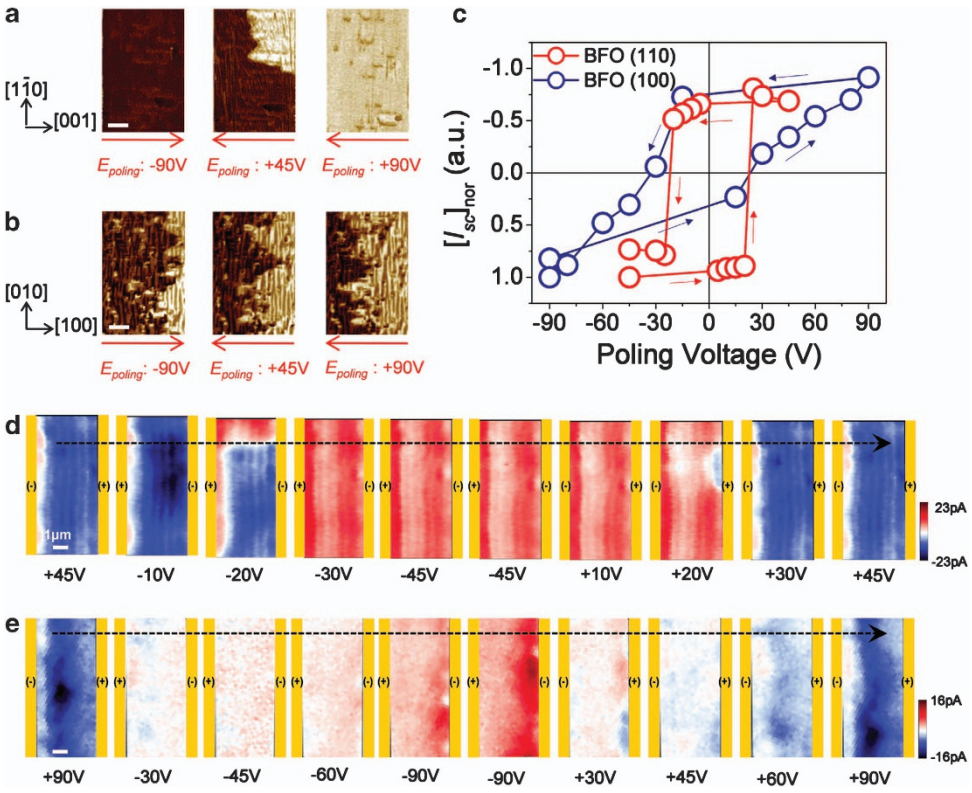

Figure 2 (**a**, **b**) In-plane piezoresponse force microscope images of the single-domain and multi-domain BFO cells after the −90 V, +45 V and −90 V poling in the [001] and [100] directions, respectively. (**c**) The magnitude of I_{sc} under global light illumination as a function of the poling field for (110) BFO single domain (blue circle) and (100) BFO multi-domains (red circle). (**d**, **e**) Series of scanning I_{sc} images of the single-domain and multidomain BFO cells after sequential electrical poling. (+)/(−) signs indicate the polarity of the biased voltages.

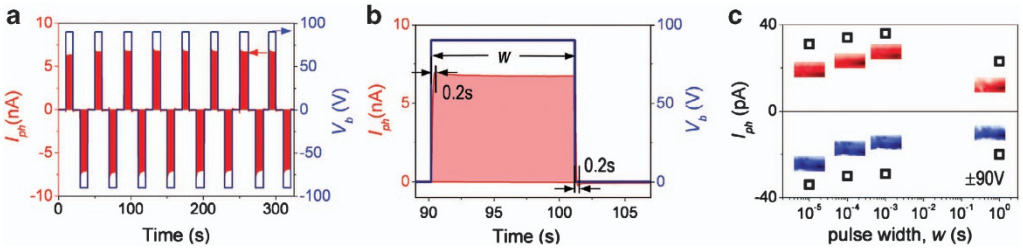

Figure 3 (**a**) Lock-in measured I_{ph} under square pulses of ±90 V in the (110) BFO single-domain cell. (**b**) A closer look at the variation in I_{ph} in response to a single square pulse of +90 V. An I_{ph} of (−)50 pA was measured after switching off the electric pulse. (**c**) I_{sc} variation under global illumination as a function of the pulse width. The insets are the scanning I_{sc} images taken immediately after each pulse was applied.

of the voltage sweep, whereas the open-circuit voltage (V_{oc}) remains constant, in clear contrast to the case of the single-domain channel. Given that the magnitude of V_{oc} is determined by the net $|\boldsymbol{P}_S|$ in the channel in the bulk photovoltaic effect model, the observed I_{sc} increase may have originated from an additional conduction contribution. We attribute this to ionic conduction by mobile oxygen vacancies, V_O^{2+}, as follows. Figure 4c shows the I_{ph} spectra taken from different spots on the single- and multidomain channels, as marked in the insets. In addition to the strong peak at 2.6–2.7 eV that corresponds to the direct band-gap absorption of BFO, the multidomain channel shows a sub-band-gap feature at 2.3 eV, whose intensity is stronger at the polar boundary and near the (−) biased electrode.[8] This non-homogeneous distribution of the sub-band-gap feature can be understood by considering the equilibrium distribution of V_O^{2+} by drift and diffusion.[20,21] To further address the role of V_O^{2+} migration in photovoltaic switching, we performed similar I_{sc}-scanning measurements at a lower temperature of 77 K, where V_O^{2+} migration can be effectively quenched.[22] According to the Nernst–Einstein relation, we note that the diffusivity of V_O^{2+} can vary by many orders of magnitude for the typical activation energy of ~1.0 eV of various perovskite oxides.[23,24] In Figures 5a and c, we show that the single-domain switching and the related photovoltaic characteristics remained qualitatively unchanged, regardless of the *E*-field poling temperatures. We only observed a small increase in I_{ph} at 300 K. In the multidomain channel, however, domain reversal became notably inhomogeneous at 77 K, as shown in Figure 5b, leading to the absence of photovoltaic characteristics, as shown in Figure 5d. This observation strongly suggests that these V_O^{2+} ions

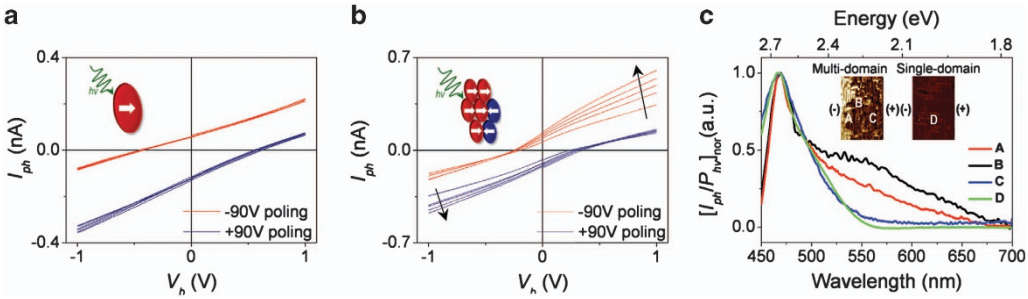

Figure 4 (**a**, **b**) Photovoltaic I_{ph}-V characteristics under global illumination in (110) BFO single-domain and (100) BFO multidomain cells during the ±90 V sweep repetition. The voltage sweep rate was 300 mV sec^{-1}. (**c**) Local spectral photoresponses under the short-circuit condition taken from the regions marked A, B, C (multidomain), and D (single domain). (+)/(−) sign indicates the polarity of the applied *E*-field.

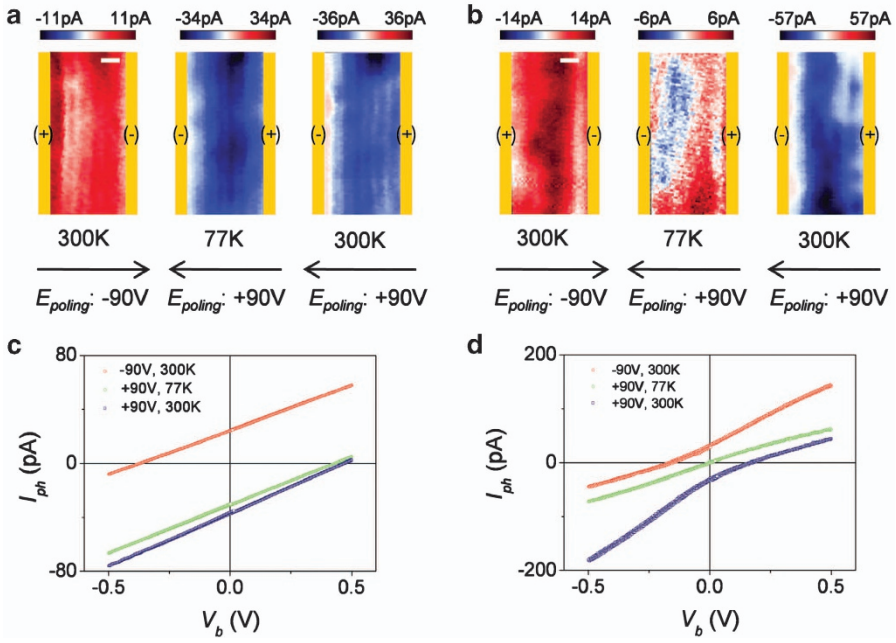

Figure 5 (**a**, **b**) Scanning I_{sc} images of the (110) BFO single domain and (100) BFO multidomains after the ±90 V poling at 300 and 77 K, respectively. (**c**, **d**) Photovoltaic I_{ph}-V characteristics under global illumination in the (110) BFO single domain and (100) BFO multidomains under the same poling conditions indicated in (**a**, **b**).

presumably accumulated at the DWs and impede the DW motions required for domain reversal.[25,26] In perovskite oxides, it is known that mobile V_O^{2+} ions tend to occupy thermodynamically preferential sites in extended crystal defects, such as DWs, grain boundaries and dislocations.[27–34] Often, these vacancies modify local cation valences and displacements and act as wall-pinning centers.[35] In turn, they contribute to diffusive photovoltaic switching in our multidomain BFO channels, as shown in Figures 5b and d. As a result, in the multidomain channel, the switching was activated by polarization flipping in conjunction with the electromigration of oxygen vacancies.

CONFLICT OF INTEREST

The authors declare no conflict of interest.

ACKNOWLEDGEMENTS

M.-H. Jo acknowledges the support of the Basic Science Research Program (2010-0017853), MEST-AFOSR NBIT Phase II (K20716000006-07A0400-00610), Nano Original & Fundamental Technology R&D Program, Global Frontier Research Program (2011-0031639) and ERC Program (2010-0001873) through the NRF funded by the MEST. C.-H. Yang acknowledges the support of the NRF funded by the MEST (contract no. 2010-0013528). X.M. acknowledges support from the Herchel Smith Fund.

1 Sturman, B. I. & Fridkin, V. M. *The Photovoltaic and Photorefractive Effects in Noncentrosymmetric Materials* (Gordon and Breach Science Publisher, Philadelphia, 1992).
2 Belinicher, V. I. & Sturman, B. I. The photogalvanic effect in media lacking a center of symmetry. *Sov. Phys. Usp.* **23,** 199–223 (1980).
3 Choi, T., Lee, S., Choi, Y. J., Kiryukhin, V. & Cheong, S. -W. Switchable ferroelectric diode and photovoltaic effect in $BiFeO_3$. *Science* **324,** 63–66 (2009).
4 Yang, S. Y., Seidel, J., Byrnes, S. J., Shafer, P., Yang, C. -H., Rabovaossell, M. D., Yu, P., Chu, Y. -H., Scott, J. F., Ager, III J. W., Martin, L. W. & Ramesh, R. Above-bandgap voltages from ferroelectric photovoltaic devices. *Nat. Nanotechnol.* **5,** 143–147 (2009).
5 Yang, S. Y., Martin, L. W., Byrnes, S. J., Conry, T. E., Basu, S. R., Paran, D., Reichertz, L., Ihlefeld, J., Adamo, C., Melville, A., Chu, Y. -H., Yang, C. -H., Musfeldt, J. L., Scholom, D. G., Ager, III J. W. & Ramech, R. Photovoltaic effects in $BiFeO_3$. *Appl. Phys. Lett.* **95,** 062909 (2009).
6 Alexe, M. & Hesse, D. Tip-enhanced photovoltaic effects in bismuth ferrite. *Nat. Commun.* **2,** 256 (2011).
7 Ji, W., Yao, K. & Liang, Y. C. Bulk photovoltaic effect at visible wavelength in epitaxial ferroelectric $BiFeO_3$ thin films. *Adv. Mater.* **22,** 1763–1766 (2010).

8 Lee, W. -M., Sung, J. H., Chu, K., Moya, X., Lee, D., Kim, C. -J., Mathur, N. D., Cheong, S. -W., Yang, C. -H. & Jo, M. -H. Spatially resolved photodetection in leaky ferroelectric $BiFeO_3$. *Adv. Mater.* **24,** OP49–OP53 (2012).
9 Seidel, J., Fu, D., Yang, S. Y., Alarcon-Llado, E., Wu, J., Ramesh, R. & Ager, III J. W. Efficient photovoltaic current generation at ferroelectric domain walls. *Phys. Rev. Lett.* **107,** 126805 (2011).
10 Seidel, J., Martin, L. W., He, Q., Chu, Y. -H., Rother, A., Hawkridge, M. E., Maksymovych, P., Yu, P., Gajek, M., Balke, N., Kalinin, S. V., Gemming, S., Wang, F., Catalan, G., Scott, J. F., Spaldin, N. A., Orenstein, J. & Ramesh, R. Conduction at domain walls in oxide multiferroics. *Nat. Mater.* **8,** 229–234 (2009).
11 Wang, J., Neaton, J. B., Zheng, H., Nagarajan, V., Ogale, S. B., Liu, B., Viehland, D., Vaithyanathan, V., Schlom, D. G., Waghmare, U. V., Spaldin, N. A., Rabe, K. M., Wuttig, M. & Ramesh, R. Epitaxial $BiFeO_3$ multiferroic thin film heterostructures. *Science* **299,** 1719–1722 (2003).
12 Balke, N., Gajek, M., Tagantsev, A. K., Martin, L. W., Chu, Y. -H., Ramesh, R. & Kalinin, S. V. Direct observation of capacitor switching using planar electrodes. *Adv. Funct. Mater.* **20,** 3466–3475 (2010).
13 Baek, S. H., Jang, H. W., Folkman, C. M., Li, Y. L., Winchester, B., Zhang, J. X., He, Q., Chu, Y. H., Nelson, C. T., Rzchowski, M. S., Pan, X. Q., Ramesh, R., Chen, L. Q. & Eom, C. B. Ferroelastic switching for nanoscale non-volatile magnetoelectric devices. *Nat. Mater.* **9,** 309–314 (2010).
14 Balke, N., Choudhury, S., Jesse, S., Huijben, M., Chu, Y. H., Baddorf, A. P., Chen, L. Q., Ramesh, R. & Kalinin, S. V. Deterministic control of ferroelastic switching in multiferroic materials. *Nat. Nanotechnol.* **4,** 868–875 (2009).
15 Kim, C. -J., Lee, H. -S., Cho, Y. -J., Kang, K. & Jo, M. -H. Diameter-dependent internal gain in ohmic Ge nanowire photodetectors. *Nano Lett.* **10,** 2043–2048 (2010).
16 Kim, C. -J., Lee, H. -S., Cho, Y. -J., Yang, J. -E., Lee, R. R., Lee, J. K. & Jo, M. -H. On-nanowire band-graded Si:Ge photodetectors. *Adv. Mater.* **23,** 1025–1029 (2011).
17 Scott, J. F. *Ferroelectric Memories* (Springer-Verlag, Berlin Heidelberg, 2000).
18 Zavaliche, F., Shafer, P., Ramesh, R., Cruz, M. P., Das, R. R., Kim, D. M. & Eom, C. B. Polarization switching in epitaxial $BiFeO_3$ films. *Appl. Phys. Lett.* **87,** 252902 (2005).
19 Pantel, D., Chu, Y. -H., Martin, L. W., Ramesh, R. & Hesse, D. Switching kinetics in epitaxial $BiFeO_3$ thin films. *J. Appl. Phys.* **107,** 084111 (2010).
20 Blanc, J. & Staebler, D. L. Electrocolaration in $SrTiO_3$: vacancy drift and oxidation-reduction of transition metals. *Phys. Rev. B* **4,** 3548–3557 (1971).
21 Yoo, H. -I., Chang, M. -W., Oh, T. -S., Lee, C. -E. & Becker, K. D. Electrocoloration and oxygen vacancy mobility of $BaTiO_3$. *J. Appl. Phys.* **102,** 093701 (2007).
22 Yi, H. T., Choi, T., Choi, S. G., Oh, Y. S. & Cheong, S. -W. Mechanism of the switchable photovoltaic effect in ferroelectric $BiFeO_3$. *Adv. Mater.* **23,** 3403–3407 (2011).
23 Yang, C. -H., Seidel, J., Kim, S. Y., Rossen, P. B., Yu, P., Gajek, M., Chu, Y. H., Martin, L. W., Holcomb, M. B., He, Q., Maksymovych, P., Balke, N., Kalinin, S. V., Baddorf, A. P., Basu, S. R., Scullin, M. L. & Ramesh, R. Electric modulation of conduction in multiferroic Ca-doped $BiFeO_3$ films. *Nat. Mater.* **8,** 485–493 (2009).
24 Menzel, S., Waters, M., Marchewka, A., Böttger, U., Dittmann, R. & Waser, R. Origin of the ultra-nonlinear switching kinetics in oxide-based resistive switches. *Adv. Funct. Mater.* **21,** 4487–4492 (2011).
25 He, L. & Vanderbilt, D. First-principles study of oxygen-vacancy pinning of domain walls in $PbTiO_3$. *Phys. Rev. B* **68,** 134103 (2003).
26 Scott, J. F. & Dawber, M. Oxygen-vacancy ordering as a fatigue mechanism in perovskite ferroelectrics. *Appl. Phys. Lett.* **76,** 3801–3803 (2000).
27 Muller, D. A., Nakagawa, N., Ohtomo, A., Grazul, J. L. & Hwang, H. Y. Atomic-scale imaging of nanoengineered oxygen vacancy profiles in $SrTiO_3$. *Nature* **430,** 657–661 (2004).
28 Jia, C. L. & Urban, L. K. Atomic-resolution measurement of oxygen concentration in oxide materials. *Science* **303,** 2001–2004 (2004).
29 Shilo, D., Ravichandran, G. & Bhattacharya, K. Investigation of twin-wall structure at the nanometre scale using atomic force microscopy. *Nat. Mater.* **3,** 453–457 (2004).
30 Szot, K., Speier, W., Bihlmayer, G. & Waser, R. Switching the electrical resistance of individual dislocations in single-crystalline $SrTiO_3$. *Nat. Mater.* **5,** 312–320 (2006).
31 Basletic, M., Maurice, J. -L., Carretero, C., Herranz, G., Copie, O., Bibes, M., Jacquet, E., Bouzehouane, K., Fusil, S. & Barthelemy, A. Mapping the spatial distribution of charge carriers in $LaAlO_3/SrTiO_3$ heterostructures. *Nat. Mater.* **7,** 621–625 (2008).
32 Kim, M., Duscher, G., Browning, N. D., Sohlberg, K., Pantelides, S. T. & Pennycook, S. J. Nonstoichiometry and the electrical activity of grain boundaries in $SrTiO_3$. *Phys. Rev. Lett.* **86,** 4056–4059 (2001).
33 Jesse, S., Rodriguez, B. J., Choudhury, S., Baddorf, A. P., Vrejoiu, I., Hesse, D., Alexe, M., Eliseev, E. A., Morozovska, A. N., Zhang, J., Chen, L. -Q. & Kalinin, S. V. Direct imaging of the spatial and energy distribution of nucleation centres in ferroelectric materials. *Nat. Mater.* **7,** 209–215 (2008).
34 Park, C. H. & Chadi, D. J. Microscopic study of oxygen-vacancy defects in ferroelectric perovskites. *Phys. Rev. B* **57,** R13961–R13964 (1998).
35 Wu, X. & Vanderbilt, D. Theory of hypothetical ferroelectric superlattices incorporating head-to-head and tail-to-tail 180° domain walls. *Phys. Rev. B* **73,** R020103 (2006).